SCIENTIFIC CULTURE
www.sci-cult.com

SCIENTIFIC CULTURE, Vol. 12, No. 1, (2026),pp.5317-5340
Open Access. Online & Print

DOI: 10.5281/zenodo.11042543

TERRAIN, LITHOLOGY AND STRUCTURAL HETEROGENEITY AS CONTROLS ON DRAINAGE NETWORK: A COMPARATIVE STUDY FROM GONDIA AND GADCHIROLI DISTRICTS, CENTRAL INDIA

Gunwant G. Wadpalliwar[1*], Shrutika R. Kamble[2], Rajni Kant[3], Shailendra G. Bommanwar[4], Sadhana S. Kambale[5], Sapana P. Titirmare[6], Ankit Surtekar[7], Riya K. Kapkar[8]

[1]Shri. Govindrao Munghate Arts and Science College Kurkheda District Gadchiroli. Email ID: ggwadpalliwar@gmail.com*
[2]Shri. Govindrao Munghate Arts and Science College Kurkheda District Gadchiroli
[3]Ballarpur Institute of Technology Bamhani, Ballarpur Diststrict: Chandrapur
[4]Ballarpur Institute of Technology Bamhani, Ballarpur Diststrict: Chandrapur
[5]Shri. Govindrao Munghate Arts and Science College Kurkheda District Gadchiroli
[6]Mahatma Gandhi Arts Science and late N P commerce College Armori, Distric Gadchiroli
[7]School of Earth Sciences, Swami Ramanand Teerth Maratwada University, Nanded
[8]th from Groundwater Survey and Development Agency District: Gadchiroli

Received: 01/12/2025
Accepted:02/01/2026

ABSTRACT

Drainage network organization in Gondia and Gadchiroli was interpreted as the outcome of interacting relief, lithological variability, weathering and mapped structural discontinuities. Through GIS-based analysis, a wider elevation range, steeper relief and a substantially longer drainage network were identified in Gadchiroli than in Gondia. However, closely comparable drainage densities of 1.179 and 1.160 km km^{-2} were obtained, respectively, indicating that the larger network in Gadchiroli was related primarily to its greater spatial extent rather than to markedly greater channel concentration. Approximately three quarters of the total segment count and drainage length in both districts were contributed by first and second order streams, by which broadly similar hierarchical organization was demonstrated. Archean gneiss, migmatite and Dongargarh Granite were identified as the dominant drainage bearing lithologies. Strong associations with Dongargarh Granite were recorded for Sati and Khobragadi, whereas Kathani, Pal and Kolandi were aligned mainly across granite and gneiss. The greatest lithological heterogeneity was observed along Gadhavi. Substantially greater dyke density and drainage–dyke crossing frequency were identified in entire Gadchiroli and Gondiya District, whereas normalized fault crossing rates were found to be comparatively similar between the districts. The highest dyke crossing rates were recorded along Bandia and Sati, the highest normalized fault crossing rate was obtained for Gadhavi and shear zone intersections were distinguished along Khobragadi. Drainage development was therefore interpreted as being jointly influenced by terrain, lithology and structural heterogeneity, while the mapped crossings were treated as spatial associations rather than as proof of tectonic control or quantified groundwater recharge.

KEYWORDS: drainage morphometry; lithological control; structural discontinuities; river–structure intersections; hard-rock terrain.

Copyright: © 2026. This is an open-access article distributed under the terms of the Creative Commons Attribution License. (https://creativecommons.org/licenses/by/4.0/).

1. INTRODUCTION

Drainage networks are commonly regarded as integrated landscape responses to terrain, lithology, geological structures, weathering and long-term erosional processes. The direction, density and hierarchical organization of channels are controlled not only by topographic gradients but also by differences in rock resistance, fracture development, regolith thickness and structural discontinuities. Important spatial evidence of the geological and geomorphometric conditions under which surface runoff is collected and routed can therefore be provided by drainage patterns.

Consistent analysis of drainage organization over extensive regions has been enabled by digital elevation models and geographic information systems. Elevation, slope, flow direction and flow accumulation can be derived from raster terrain data, while drainage networks can be extracted and classified through standardized hydrological procedures. The D8 flow-routing method developed by O'Callaghan and Mark (1984) continues to be widely applied for the identification of downslope flow paths. Terrain conditioning, drainage extraction and stream ordering within reproducible GIS workflows are further supported by Whitebox-based geomorphometric tools (Lindsay, 2016).

The reliability of a derived drainage network is nevertheless affected by DEM resolution, hydrological preprocessing and the selected flow-accumulation threshold. Near-global elevation information at approximately one-arc-second resolution is provided by NASADEM and can be applied to regional terrain and drainage analysis (NASA Jet Propulsion Laboratory, 2020). However, natural flow paths may be interrupted by depressions, flat surfaces and elevation artefacts, which must be addressed before drainage extraction. Dense networks containing numerous headwater channels are generally produced by smaller accumulation thresholds, whereas only more strongly accumulated flow paths are retained by larger thresholds. Drainage density, stream number and maximum stream order must therefore be interpreted within the adopted DEM resolution and extraction framework (Shekar & Mathew, 2024).

Valuable regional context for river-network analysis is provided by global hydrographic products. Improved representation of basin connectivity and drainage pathways at broad spatial scales has been achieved through HydroSHEDS, MERIT Hydro and Hydrography90m (Lehner & Grill, 2013; Yamazaki et al., 2019; Amatulli et al., 2022). Spatially variable drainage density has also been incorporated into global vector river datasets (Lin et al., 2021). However, every headwater, seasonal or locally named channel cannot be represented consistently by global products. River-network geometry and completeness have therefore been improved through multi-source fusion and satellite-based waterway mapping (Liu et al., 2026; Pierson & Mehrabi, 2024). At the district scale, locally processed DEM data are generally considered more suitable for the calculation of drainage length, stream order and drainage density.

An additional source for the identification of named rivers and approximate channel alignments is provided by OpenStreetMap. Its principal value is associated with the preservation of local river identity where DEM-derived channels remain unnamed. However, spatial and temporal variation is observed in OpenStreetMap completeness and positional accuracy, and waterways may be fragmented, generalized or displaced (Monteiro & Patrício, 2024). A complementary approach is therefore required, under which river identification is supported by OpenStreetMap and the quantitative analytical network is provided by DEM-derived drainage.

Drainage development may be influenced by lithological differences in mineral composition, rock strength, weathering susceptibility, jointing and regolith formation. Ridges and elevated surfaces may be preserved by resistant geological units, whereas greater channel incision may be permitted by weathered or mechanically weakened rocks. Channel orientation may also be influenced by faults, shear zones, fractures and intrusive contacts through the creation of zones of weakness or contrasting erosion resistance. However, structural control cannot be demonstrated independently by a spatial intersection between a river and a mapped structure. Crossing frequency must instead be interpreted in relation to drainage length, structural abundance and the numerical dominance of lower-order streams.

These relationships are especially relevant to Gondia and Gadchiroli districts in eastern Maharashtra. Within the study area, a heterogeneous crystalline and metamorphic geological framework is represented by Archean gneiss, migmatite and Dongargarh Granite, metavolcanic rocks, sedimentary and iron-bearing formations, quartzite, schist, amphibolite and localized intrusive units. The geological terrain is additionally intersected by mapped faults, shear zones and numerous mafic dykes. S.B. Deshmukh., et al (2023). Five rivers Bandia, Gadhavi, Kathani, Khobragadi and Sati—were selected for study.

Possible implications for groundwater recharge may also be associated with terrain, drainage and geological conditions. In hard-rock regions, groundwater storage and movement are generally controlled by secondary porosity developed through weathering, fractures, joints and structurally weakened zones. Infiltration may potentially be supported by valley settings, low-gradient surfaces, weathered granitoid terrain and hydraulically connected fractures. Conversely, rapid surface-water transfer may be promoted by steep slopes, while subsurface movement may be locally restricted by massive mafic dykes. Nevertheless, groundwater

recharge cannot be quantified from drainage density, lithology or structural crossings alone, and additional rainfall, soil, regolith, groundwater-level and aquifer-property data are required. Groundwater implications were therefore considered conceptually rather than through recharge modelling or groundwater-potential zonation.

Drainage morphometry, geological mapping, structural interpretation and groundwater conditions have commonly been examined as separate components in previous studies. Integration of DEM-derived drainage, lithology-normalized drainage density, mapped structural density and length-normalized river–structure crossings has been undertaken in comparatively few district-scale investigations. Moreover, geological control is sometimes inferred from visual correspondence without river length, structural abundance or extraction-scale effects being adequately considered.

Accordingly, an integrated GIS-based assessment was undertaken to prepare district wide drainage and geological maps, characterize terrain and drainage organization, and evaluate lithological and structural associations across Gondia and Gadchiroli. Because a validated geomorphological dataset was unavailable, the geomorphological setting was represented through DEM-derived elevation, slope, hillshade and contour analyses rather than through a formal classified geomorphology map.

The relationships between district-scale drainage organization, lithological variability and mapped geological structures in Gondia and Gadchiroli were evaluated through an integrated GIS-based terrain and geological framework.

Objectives

- To prepare district wide drainage and geological maps of Gondia and Gadchiroli using NASADEM, named river reference data and compiled lithological and structural datasets.
- To characterize the terrain and geomorphometric setting of the two districts using elevation, slope, hillshade, contours, drainage density and Strahler stream-order analysis.
- To evaluate the role of lithology in drainage development by comparing drainage length and drainage density across mapped geological units and by examining lithological associations along the Bandia, Gadhavi, Kathani, Khobragadi and Sati rivers.
- To assess the spatial association between drainage and geological structures by quantifying mapped fault, shear-zone and dyke densities and calculating raw and length-normalized structural-crossing rates.
- To discuss the possible implications of terrain, lithology and structural discontinuities for groundwater recharge, while distinguishing conceptual hydrogeological interpretation from directly measured recharge or groundwater-potential evidence.

2. LITERATURE REVIEW

2.1 DEM-Based Terrain and Drainage-Network Extraction

A consistent basis for representing elevation, slope, flow direction and flow accumulation is provided by digital elevation models (DEMs). The D8 method introduced by O'Callaghan and Mark (1984) continues to be widely applied for routing flow between neighbouring raster cells and extracting drainage networks. Near-global elevation data at approximately one-arc-second resolution are provided by NASADEM, in which improvements to the original SRTM product have been incorporated (NASA Jet Propulsion Laboratory, 2020). However, automated routing may be disrupted by flat terrain, artefacts and artificial depressions.

Hydrological conditioning is therefore required before drainage extraction. Depressions may be filled or breached, while flow direction, accumulation, stream extraction and ordering can be implemented through Whitebox geospatial tools (Lindsay, 2016). Network density is also controlled by the selected flow-accumulation threshold: more headwater channels are retained by smaller thresholds, whereas only strongly accumulated paths are preserved by larger thresholds. Stream count, channel length, drainage density and maximum stream order should therefore be compared only when DEM resolution and extraction settings have been kept consistent (Shekar & Mathew, 2024). Drainage hierarchy is commonly represented through the Strahler system (Strahler, 1957).

2.2 Global Hydrography and Multi-Source River Representation

Standardized representations of rivers and basin connectivity are provided by global hydrographic datasets. Basin delineation and network routing are supported by HydroSHEDS (Lehner & Grill, 2013), while corrected topography and water-body information are incorporated into MERIT Hydro (Yamazaki et al., 2019). Improved representation of smaller drainage pathways is provided by Hydrography90m (Amatulli et al., 2022), whereas spatially variable drainage density was incorporated by Lin et al. (2021).

Nevertheless, every local or seasonal channel cannot be represented consistently by global datasets because differences in resolution and extraction rules are involved. Multi-source fusion has been applied to improve river geometry and topology (Liu et al., 2026), while waterway mapping has been supported by satellite imagery and deep learning (Pierson & Mehrabi, 2024). Regional products are therefore best treated as contextual references, whereas locally processed DEMs are considered more suitable for district-scale metrics (Hou et al., 2025).

2.3 OpenStreetMap as a Studied-River Reference

Named rivers for which DEM-derived channels remain unnamed can be identified through OpenStreetMap (OSM). However, spatial and temporal variation is observed in OSM completeness, and waterways may be fragmented, generalized, displaced

or absent (Monteiro & Patrício, 2024).

Different errors are also associated with OSM and DEM-derived networks. Cartographic generalization may be reflected by OSM lines, whereas DEM-derived channels may be affected by elevation artefacts or threshold selection. A complementary approach is therefore preferred: river naming and alignment may be supported by OSM, while calculations of stream order, channel length and drainage density should be based on DEM-derived networks.

2.4 Morphometric Interpretation in Terrain and Lithological Context

Drainage geometry is converted through morphometric analysis into indicators of channel organization and landscape dissection. These measures are widely applied to watershed characterization and conservation planning (Pande et al., 2021; Singh et al., 2023). Drainage density is calculated as total channel length divided by area; however, it is affected by relief, slope, rainfall, vegetation, soils, weathering, bedrock properties, DEM resolution and extraction threshold. It should therefore not be treated as a direct measure of permeability, runoff or recharge.

Drainage may be influenced by lithological differences in rock strength, weathering, jointing and regolith formation. Ridges may be preserved by resistant units, whereas greater incision may be permitted by weathered or structurally weakened rocks. However, similar drainage densities may be produced over contrasting rock types where bedrock differences are offset by slope, fracture density or surface materials. Lithology-specific comparisons are more meaningful when drainage length is normalized by the mapped area of each geological class. Values derived from very small areas should be interpreted cautiously because density estimates may be exaggerated by unstable denominators.

2.5 Structural Associations and Groundwater Implications

Drainage may be influenced by faults, shear zones, fractures and intrusive contacts through mechanical weakness, erosion contrasts or localized permeability changes. Channels may be aligned with, intersect or become deflected near such structures; however, structural control cannot be demonstrated by a geometric intersection alone. Crossing frequency is also affected by structural abundance, drainage density and study-area size. Raw counts should therefore be normalized by drainage or river length, while first-order crossings require caution because lower-order streams are generally the most numerous.

Hydraulic barriers may be formed by massive and unweathered dykes, whereas preferential flow may be supported by weathered margins and fractured contacts. Groundwater circulation may be enhanced by faults and shear zones where they are open and connected, yet it may be restricted. Hydrogeological behaviour cannot therefore be determined from structural class alone.

Water-resource assessment can be supported by Geoinformatics through the integration of terrain, drainage and geology (Jagadeesha & Manavalan, 2025; Tarate et al., 2024). Nevertheless, groundwater recharge cannot be quantified from drainage density or structural intersections alone. Rainfall, soils, regolith thickness, land cover, groundwater levels and aquifer parameters are also required. Contextual interpretation may be supported by surface-water mapping, but recharge or aquifer storage cannot be measured directly from visible water occurrence (Drusch et al., 2012; Pekel et al., 2016; Xu, 2006).

2.6 Research Gap and Analytical Scope

Drainage morphometry, hydrography, geological mapping, structural interpretation and groundwater assessment are often undertaken separately. Integration of DEM derived drainage, lithology-normalized drainage density, mapped structural density and river-wise crossing rates within a single district scale framework has been attempted in relatively few studies. Geological influence is also frequently inferred from visual correspondence without normalization by river length, drainage density or structural abundance.

These limitations are addressed in the present study through the integration of NASADEM-based terrain analysis, conditioned drainage extraction, Strahler ordering, generalized lithological mapping, structural-density assessment and river analysis across Gondia and Gadchiroli. Drainage density is compared among mapped lithological units, while fault, shear-zone and dyke intersections are evaluated using raw and length-normalized rates. Groundwater implications are discussed conceptually rather than as measured recharge or groundwater-potential results, thereby preserving the distinction between mapped association and field-validated geological or hydrogeological causation.

3. METHODOLOGY

The overall methodological workflow adopted for the study is presented in Figure 1. Spatial-data collection and terrain processing were followed by drainage-network extraction, geological and structural integration, and quantitative spatial assessment. The resulting maps and metrics were then used for the interpretation of terrain–drainage relationships, lithological and structural associations, and possible groundwater-recharge implications. Comprehensive geological, geomorphological, and hydrogeological field investigations were conducted throughout the study area to validate the datasets generated from Remote Sensing and GIS (Fig: 9: a, b, c, d, e, and f)

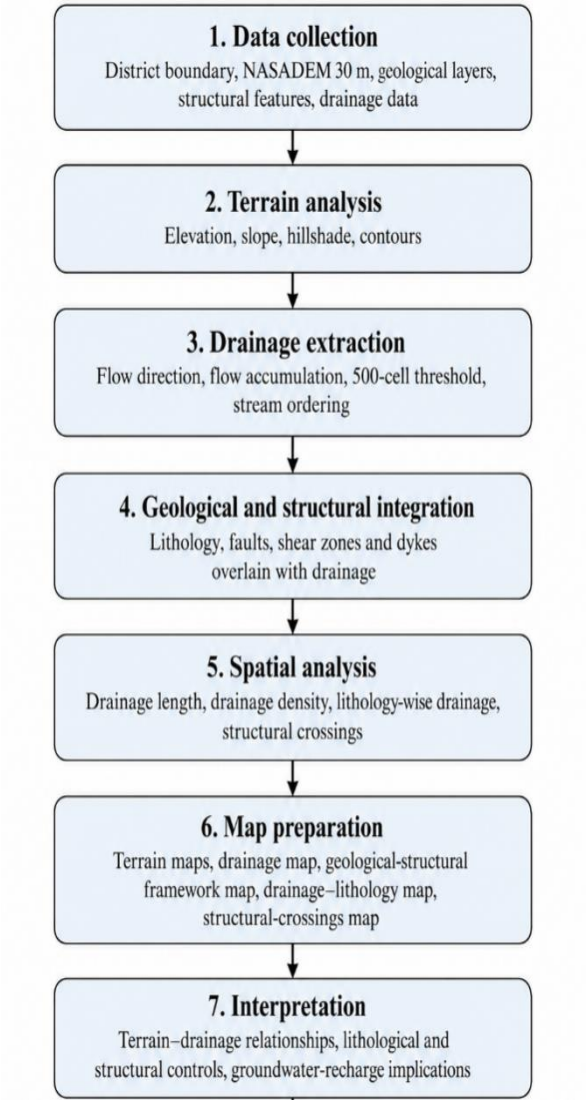


Figure 1. Methodological workflow for the GIS-based assessment of terrain, drainage, lithological and structural relationships in Gondia and Gadchiroli districts.

3.1 Study Area and Spatial Data Sources

The study was conducted across Gondia and Gadchiroli districts in easternmost Maharashtra, India. Based on the projected administrative boundaries, the districts cover approximately 5,471.79 km^2 and 14,447.81 km^2, respectively. The study region is characterized by heterogeneous terrain, well-developed drainage networks and substantial geological variability. Elevation, slope, lithology and mapped structural discontinuities were therefore considered jointly to evaluate the spatial organization of the drainage system.

Geologically, the region forms part of the broader Bastar Craton and contains extensive exposures of Gneiss and Granite, volcanic and metavolcanic rocks, sedimentary formations, quartzite, schist, amphibolite and younger surficial deposits. The mapped structural framework includes faults, shear zones and numerous intrusive dykes. Five rivers Bandia, Gadhavi, Kathani, Khobragadi and Sati were selected for river-specific lithological and structural analyses.

Administrative boundaries were used for study-area delineation, spatial clipping and district-level aggregation. Terrain information was obtained from the 30 m NASADEM and was used to derive elevation, slope, hillshade, contours, flow direction, flow accumulation and drainage networks. Geological polygons and mapped faults, shear zones and dykes were obtained from the available Geological Survey of India, NGDR geological datasets. Named river geometries were extracted from OpenStreetMap waterway data and were subsequently standardized and clipped to the study boundaries.

All datasets were inspected for coordinate-system consistency, geometry validity and spatial completeness. Vector and raster layers were projected to WGS 84/UTM Zone 44N (EPSG:32644) to permit area, length and density calculations in metric units. Spatial processing was performed using QGIS and WhiteboxTools, while tabulation, validation, visualization and statistical aggregation were conducted using Python libraries, including GeoPandas, Pandas, Shapely and Matplotlib. Areas without available geological polygons were retained as unmapped geological coverage and were not assigned inferred

lithological classes.

3.2 Terrain Analysis and Drainage-Network Extraction

The NASADEM was first projected to WGS 84/UTM Zone 44N (EPSG:32644) and clipped to the combined boundary of Gondia and Gadchiroli districts. Raster integrity, elevation range and spatial alignment were checked before terrain and hydrological derivatives were generated. District-level elevation statistics, including minimum, maximum, mean and standard deviation, were calculated through zonal analysis. Slope was derived in degrees from the projected DEM, while hillshade and 50 m interval contours were produced to support interpretation of terrain variability and drainage organization.

Before drainage extraction, topographic depressions that could interrupt continuous flow routing were treated using a least-cost breaching procedure. D8 flow direction and flow accumulation rasters were subsequently generated from the hydrologically conditioned DEM. A flow-accumulation threshold of 500 cells was applied to define the district-scale drainage network. The selected threshold was intended to preserve both major channels and smaller tributary systems required for lithological and structural comparison.

The resulting stream raster was classified according to the Strahler ordering system and converted to vector format. Stream segments were clipped by district boundaries, and segment lengths were calculated in kilometres. For each district, the number of stream segments, total drainage length, maximum Strahler order and stream-order-specific length distribution were summarized.

Drainage density was calculated as:

$$Dd = \frac{Ld}{Ad}$$

where Dd represents drainage density in km/km^2, Ld represents the total extracted drainage length in kilometres, and Ad represents district area in square kilometres.

The final drainage layer was used as the common hydrological framework for subsequent drainage–lithology intersections, structural-crossing analysis and comparison with the five named rivers.

3.3 Geological and Structural Data Preparation

The geological datasets for Gondia and Gadchiroli were examined separately before being integrated into a common analytical framework. Invalid geometries were repaired, non-spatial records were excluded, and all layers were reprojected to WGS 84/UTM Zone 44N (EPSG:32644). The geological polygons were then clipped to the district boundaries and merged into a unified lithological layer. Polygon areas were calculated in square kilometres to support district-wise and lithology-wise normalization.

Because the source data contained numerous detailed lithological descriptions, the original attributes were standardized and consolidated into 11 generalized classes: alluvium and valley fill; laterite; sedimentary rocks and iron formations; volcanic and metavolcanic rocks; schist, phyllite and metasedimentary rocks; quartzite and meta-arkose; amphibolite and metamafic-ultramafic rocks; other high-grade metamorphic rocks; granite gneiss and migmatite; Dongargarh Granite; and other intrusive rocks and dykes. Areas without mapped geological polygons were retained as data gaps and were excluded from lithology-specific calculations.

Faults, shear zones and dykes were processed independently. Each structural layer was repaired, reprojected, clipped to the district boundaries and merged across both districts. Segment lengths were calculated in kilometres, after which the number of mapped segments, total structural length and mean segment length were summarized by district.

Structural density was calculated as:

$$Sd = \frac{Ls}{Ad}$$

where Sd denotes the mapped structural density in km/km^2, Ls represents the total mapped length of the selected structural feature, and Ad represents district area in square kilometres.

The resulting lithological and structural layers were used to prepare the geological framework map and to support subsequent drainage–lithology and drainage–structure analyses. Structural density was interpreted as the spatial concentration of mapped features rather than as an indicator of present-day tectonic activity.

3.4 Drainage–Lithology and River Analysis

The spatial relationship between drainage development and lithological variation was evaluated by intersecting the 500-cell Strahler-ordered drainage network with the generalized lithological polygons. For each district and lithological class, the mapped geological area and the cumulative drainage length were calculated. Drainage density within each lithological unit was then determined as:

$$Dd,l = \frac{Ld,l}{Ad,l}$$

where Dd,l represents drainage density for lithological class l within district d, Ld,l denotes the total drainage length intersecting that class, and Ad,l denotes its mapped area. Classes represented by very small mapped areas were identified and interpreted cautiously because their density estimates could be disproportionately influenced by limited spatial coverage.

The five rivers dataset was filtered to retain the Bandia, Gadhavi, Kathani, Khobragadi and Sati rivers. River names were standardized, multipart geometries were retained where district boundaries divided a river, and the total length of each river was calculated in kilometres. Each river was subsequently intersected with the lithological layer to quantify the length associated with individual geological classes.

The proportional contribution of each lithology to the mapped river length was calculated as:

$$Pr,l = \frac{Lr,l}{Lr,m} \times 100$$

where Pr,l represents the percentage of river r associated with lithological class l, Lr,l denotes the river length within that class, and Lr,m represents the total

river length covered by mapped geology.

For each studied river, geological coverage, dominant lithology, second-ranked lithology and their respective proportional shares were identified. These metrics were used to distinguish rivers predominantly associated with a single lithological terrain from those traversing more heterogeneous geological settings. The observed associations were interpreted as spatial relationships rather than as direct evidence that lithology alone controlled river-course development.

3.5 Drainage–Structure Intersection, Normalization and Quality Control

The spatial coincidence between the drainage network and mapped structural features was assessed separately for faults, shear zones and dykes. Line-intersection analysis was applied between the 500-cell drainage network and each structural dataset, producing point features at every geometric crossing. Duplicate point geometries generated at multipart boundaries or coincident line segments were removed before statistical aggregation. Crossing counts were then summarized by district, structural class and Strahler stream order.

To account for differences in total drainage length between the two districts, district-level crossing rates were normalized as:

$$C100,d = Nc,dLd \times 100$$

where $C100,d$represents the number of crossings per 100 km of drainage, Nc,ddenotes the total number of drainage–structure intersections in district d, and Ldrepresents the district drainage length in kilometres. First-order crossing counts and the highest stream order intersected by each structural class were also determined. However, first-order results were interpreted in relation to the numerical dominance of first-order channels within the extracted network.

A separate intersection analysis was undertaken for the Bandia, Gadhavi, Kathani, Khobragadi and Sati rivers. Fault, shear-zone and dyke crossings were counted for each river and normalized by river length:

$$C100,r = Nc,rLr \times 100$$

where $C100,r$denotes structural crossings per 100 km, $Nc,r$is the number of mapped crossings along river r, and $Lr$is its total mapped length.

Quality control was applied throughout the workflow. Coordinate reference systems, geometry validity, null geometries, duplicate intersections and district-level totals were checked. Stream-order totals were reconciled with district totals, and normalized rates were independently recalculated. Areas lacking geological coverage were excluded from lithology-specific normalization. Structural intersections were interpreted as mapped spatial coincidences and not as definitive evidence of tectonic control, active faulting or contemporary channel deformation.

4. RESULTS

4.1 Terrain Characteristics and District-Scale Drainage Conditions

Considerable spatial variation in terrain was identified across Gondia and Gadchiroli districts, as demonstrated by the elevation, slope, hillshade and contour maps presented in Figures 2–4. Gondia was characterized by a higher mean elevation of 312.35 m, whereas a lower mean elevation of 249.29 m was recorded for Gadchiroli. However, a broader altitudinal range was observed in Gadchiroli, where elevations varied from 67 to 932 m, compared with 209–713 m in Gondia (Table 1).

The elevation distribution shown in Figure 2 indicated that relatively elevated terrain was concentrated across northern Gondia and in localized eastern and southeastern sectors of the study area. Lower elevations were distributed mainly across the western, central and south-central portions of Gadchiroli. Although the district-wide mean elevation was lower in Gadchiroli, several isolated uplands and ridge systems attained elevations greater than those observed across most of Gondia.

Slope conditions were dominated by nearly level and gently sloping surfaces across substantial portions of both districts (Figure 3). Localized moderate, steep and very steep slopes were concentrated along ridges, dissected uplands and escarpment-like terrain. A mean slope of 4.09° was recorded in Gadchiroli, compared with 3.50° in Gondia. Maximum slope values of 69.49° and 52.61° were recorded in Gadchiroli and Gondia, respectively. Greater localized relief and steeper terrain were therefore represented in Gadchiroli despite its lower mean elevation.

The hillshade and contour patterns shown in Figure 4 further demonstrated the contrast between subdued surfaces and topographically dissected sectors. Closely spaced contours were observed along elevated ridges and steep slopes, particularly in eastern and southern Gadchiroli and in selected parts of northern and central Gondia. Wider contour spacing was associated with comparatively low-relief terrain. Elevations exceeding approximately 500–600 m were restricted mainly to localized upland sectors rather than being continuously distributed across either district.

A total drainage length of 17,032.19 km was extracted within Gadchiroli, compared with 6,346.61 km in Gondia. The greater drainage length recorded in Gadchiroli corresponded primarily to its larger geographical area of 14,447.81 km^2, compared with 5,471.79 km^2 for Gondia. Despite the substantial difference in absolute drainage length, similar drainage-density values were obtained for the two districts. Drainage densities of 1.179 km/km^2 and 1.160 km/km^2 were recorded for Gadchiroli and Gondia, respectively. Broadly comparable district-scale channel concentrations were therefore identified, although the drainage network in Gadchiroli was distributed across a larger and more topographically variable landscape

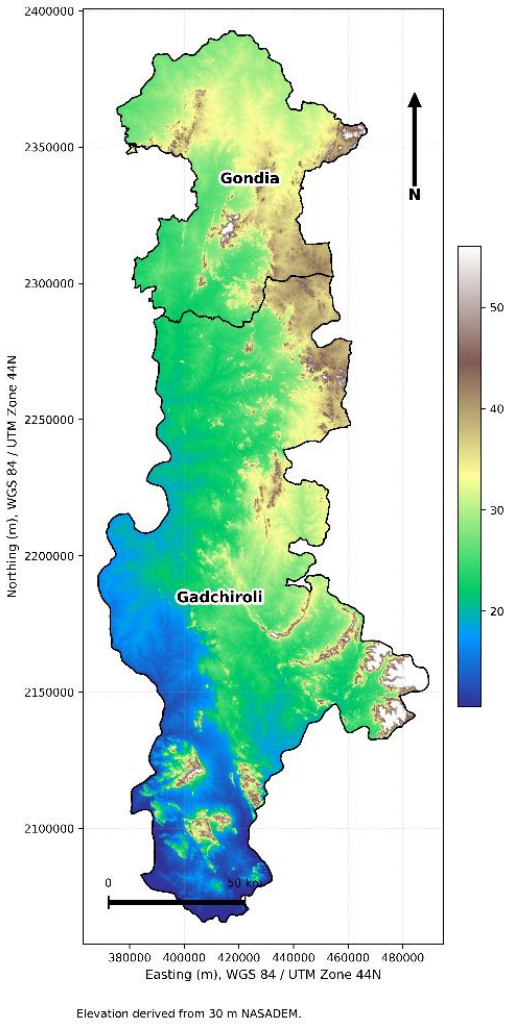


Figure 2. Elevation distribution across Gondia and Gadchiroli districts, derived from the 30 m NASADEM.

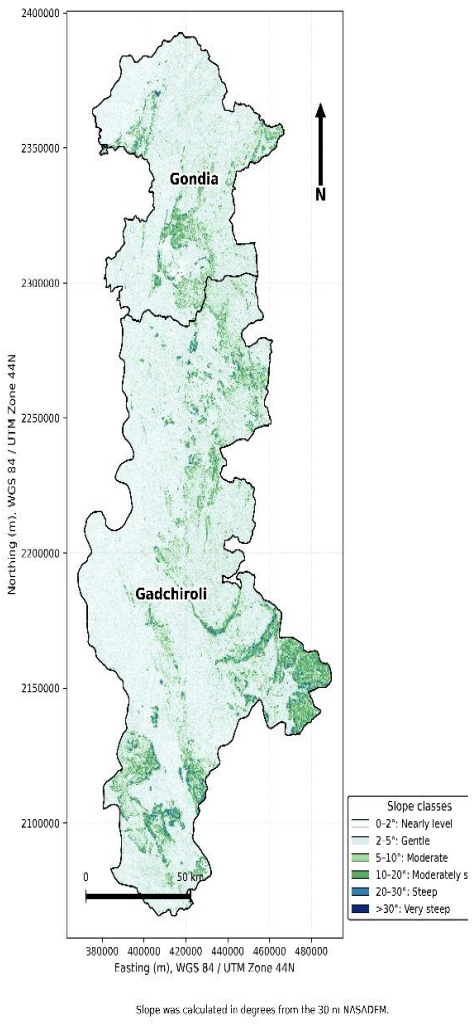


Figure 3. Spatial distribution of slope classes across Gondia and Gadchiroli districts, derived in degrees from the 30 m NASADEM.

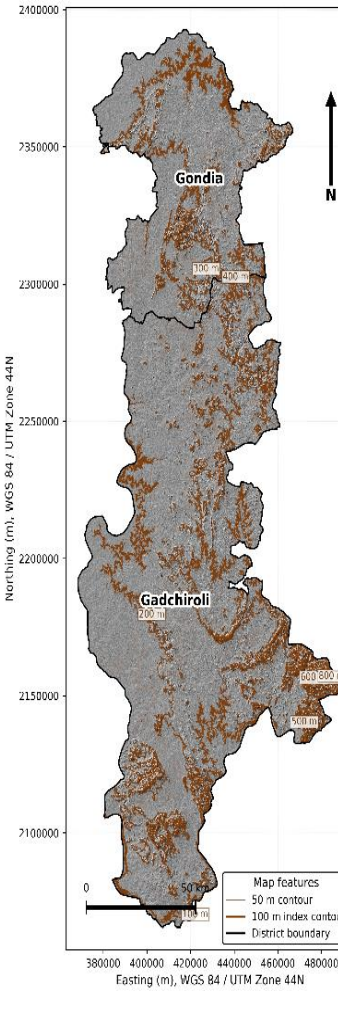


Figure 4. Hillshade and topographic contours of Gondia and Gadchiroli districts, with contours displayed at 50 m intervals and 100 m index contours emphasized.

Table 1. Terrain and district-scale drainage characteristics of Gondia and Gadchiroli

District	Area (km²)	Mean elevation (m)	Minimum elevation (m)	Maximum elevation (m)	Mean slope (°)	Maximum slope (°)	Drainage segments	Total drainage length (km)	Maximum Strahler order	Drainage density (km/km²)
Gadchiroli	14,447.81	249.29	67	932	4.09	69.49	18,209	17,032.19	8	1.179
Gondia	5,471.79	312.35	209	713	3.50	52.61	6,781	6,346.61	7	1.160

The principal terrain and drainage characteristics of the two districts are summarized in Table 1. Greater relief variation and a substantially longer drainage network were identified in Gadchiroli, whereas district-scale drainage density was found to remain broadly comparable with Gondia.

4.2 Drainage-Network Hierarchy and Studied Rivers

A dense and hierarchically organized drainage network was extracted across Gondia and Gadchiroli districts using the 500-cell flow-accumulation threshold. The spatial configuration of the network and the five studied rivers Bandia, Gadhavi, Kathani, Khobragadi and Sati—is presented in Figure 5. A greater absolute number of drainage segments was recorded in Gadchiroli because of its larger geographical extent, whereas a broadly comparable lower-order stream structure was observed in both districts.

A maximum Strahler order of 8 was reached by the extracted drainage network in Gadchiroli, compared with 7 in Gondia. In Gadchiroli, 18,209 stream segments were identified, of which 9,198 were classified as first order. Of the mapped segments and total drainage length, 50.51% and 50.12%, respectively, were represented by these first-order channels. A further 4,361 second-order segments were identified, representing 23.95% of the segment count and 26.48% of the drainage length (Table 2). Consequently, 74.46% of all segments and 76.60% of the extracted drainage length in Gadchiroli were represented collectively by first- and second-order channels.

A comparable distribution was obtained for Gondia. Of the 6,781 extracted stream segments, 3,443 were classified as first order and 1,616 as second order. First-order channels accounted for 50.77% of the segment count and 49.75% of the total drainage length, whereas 23.83% of the segments and 26.47% of the channel length were represented by second-order channels. Together, 74.61% of the stream segments and 76.22% of the total drainage length in Gondia were represented by these two orders.

A progressive reduction in both segment number and cumulative channel length was observed with increasing Strahler order. In Gadchiroli, only 15 eighth-order segments were identified, contributing approximately 12.18 km or 0.07% of the total drainage length. In Gondia, the highest order was represented by 35 seventh-order segments, with a cumulative length of approximately 18.24 km. The predominance of lower-order channels and the limited contribution of the highest-order streams reflected the convergent organization of the drainage networks, in which numerous headwater tributaries were progressively integrated into fewer trunk channels.

The studied river network was represented across districts but was concentrated mainly within Gadchiroli. The longest mapped river alignment was represented by Bandia, with a total length of approximately 138.27 km. This was followed by Khobragadi at 79.89 km, Gadhavi at 68.49 km, Sati at 49.03 km and Kathani at 44.42 km. Gadhavi was the only river represented across both districts, whereas the remaining mapped river alignments occurred primarily within Gadchiroli.

The closely comparable first- and second-order proportions were interpreted as evidence of similar drainage-network hierarchies in the two districts despite differences in area, relief and geological composition. However, a more extensive district-scale drainage system and a greater degree of tributary integration were indicated in Gadchiroli by the larger number of higher-order channels.

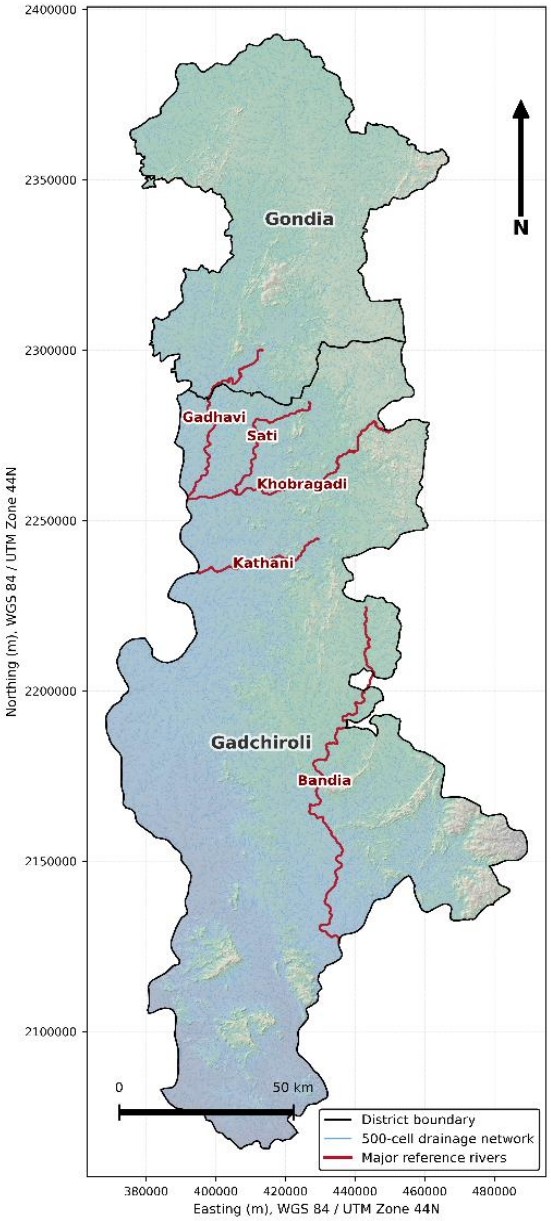


Figure 5. Strahler-ordered drainage network and studied rivers of Gondia and Gadchiroli districts.

Table 2. Strahler-order distribution of the extracted drainage network

District	Strahler order	Segment count	Total length (km)	Segment share (%)	Length share (%)
Gadchiroli	1	9,198	8,537.28	50.51	50.12
Gadchiroli	2	4,361	4,509.55	23.95	26.48
Gadchiroli	3	2,193	2,018.31	12.04	11.85
Gadchiroli	4	1,218	1,014.24	6.69	5.95
Gadchiroli	5	723	553.74	3.97	3.25
Gadchiroli	6	414	326.57	2.27	1.92
Gadchiroli	7	87	60.34	0.48	0.35
Gadchiroli	8	15	12.18	0.08	0.07
Gondia	1	3,443	3,157.60	50.77	49.75
Gondia	2	1,616	1,679.98	23.83	26.47
Gondia	3	932	859.50	13.74	13.54
Gondia	4	514	447.21	7.58	7.05
Gondia	5	202	160.67	2.98	2.53
Gondia	6	39	23.42	0.58	0.37
Gondia	7	35	18.24	0.52	0.29

The complete Strahler-order distribution is presented in Table 2. A progressive decline in segment count and cumulative channel length was observed with increasing stream order, while both district networks were dominated by first- and second-order channels.

4.3 Geological and Structural Framework

A heterogeneous geological framework was identified across Gondia and Gadchiroli districts, with crystalline basement rocks represented as the dominant mapped units (Figure 6). Extensive areas in both districts were occupied by granite and gneiss, whereas a more prominent distribution of Dongargarh Granite was recorded across Gadchiroli. metavolcanic rocks, sedimentary rocks and iron formations, quartzite, schist, amphibolite and other high-grade metamorphic units were represented as comparatively localized belts and discontinuous geological domains. (Gunwant G. Wadpalliwar,et al 2024)

Within Gadchiroli, the largest mapped lithological class was represented by granite and gneiss, which covered approximately 5,873.42 km^2 or 40.89% of the available geological coverage. The second-largest mapped unit was represented by Dongargarh Granite, which extended across approximately 4,814.05 km^2 or 33.51%. A further 1,915.06 km^2, equivalent to 13.33% of the mapped geological area, was occupied by sedimentary rocks and iron formations. Less than 5% of the mapped district area was occupied individually by each remaining lithological class.

A comparable dominance of granite gneiss, migmatite was recorded in Gondia, where approximately 2,191.31 km^2 or 43.41% of the mapped geological area was covered by this unit. The second-largest class was represented by volcanic and metavolcanic rocks, which covered 1,274.61 km^2 or 25.25%, whereas approximately 719.25 km^2 or 14.25% was occupied by Dongargarh Granite. Sedimentary rocks and iron formations accounted for 9.63% of the mapped geological area. A greater proportional representation of volcanic and metavolcanic rocks was therefore observed in Gondia than in Gadchiroli.

The structural framework was represented by mapped faults, shear zones and dykes. The most numerous and spatially extensive structural class, particularly in Gadchiroli, was represented by dykes (Table 3). In Gadchiroli, 1,873 dyke segments with a cumulative mapped length of 1,563.60 km were recorded, from which a mapped dyke density of 0.1082 km/km^2 was obtained. In contrast, only 55 dyke segments were recorded in Gondia, with a total length of 61.09 km and a density of 0.0112 km/km^2. A substantially greater dyke density was therefore recorded in Gadchiroli.

Faults were recorded less frequently than dykes but were represented by longer average segments. In Gadchiroli, 145 fault segments were identified, with a cumulative length of 382.37 km and a mapped density of 0.0265 km/km^2. In Gondia, 25 fault segments extending for 130.22 km were recorded, corresponding to a density of 0.0238 km/km^2. Although a considerably greater absolute fault length was recorded in Gadchiroli, comparatively similar normalized fault densities were obtained for the two districts.

The least numerous mapped structural category was represented by shear zones. Twenty shear-zone segments with a total length of 151.13 km were recorded in Gadchiroli, whereas six segments extending for 34.64 km were identified in Gondia. Corresponding mapped densities of 0.0105 and 0.0063 km/km^2 were obtained, respectively. Mean segment lengths of 7.56 km in Gadchiroli and 5.77 km in Gondia indicated that longer individual segments were generally represented by shear zones than by dykes or faults.

A spatially uneven structural distribution was mapped. Dense dyke concentrations were observed across large parts of Gadchiroli, whereas a more limited and discontinuous dyke pattern was represented in Gondia. Faults and shear zones were mapped across both districts but were concentrated along selected geological contacts and structurally complex zones. A more densely mapped intrusive and discontinuity framework, particularly with respect to dykes, was therefore indicated in Gadchiroli by the structural dataset.

The distribution and density of structures contained in the compiled geological database are represented by these measurements. They were not interpreted as indicators of present-day tectonic activity, and the differences between districts may partly be attributed to geological exposure, source-map scale and spatial variation in mapping detail.

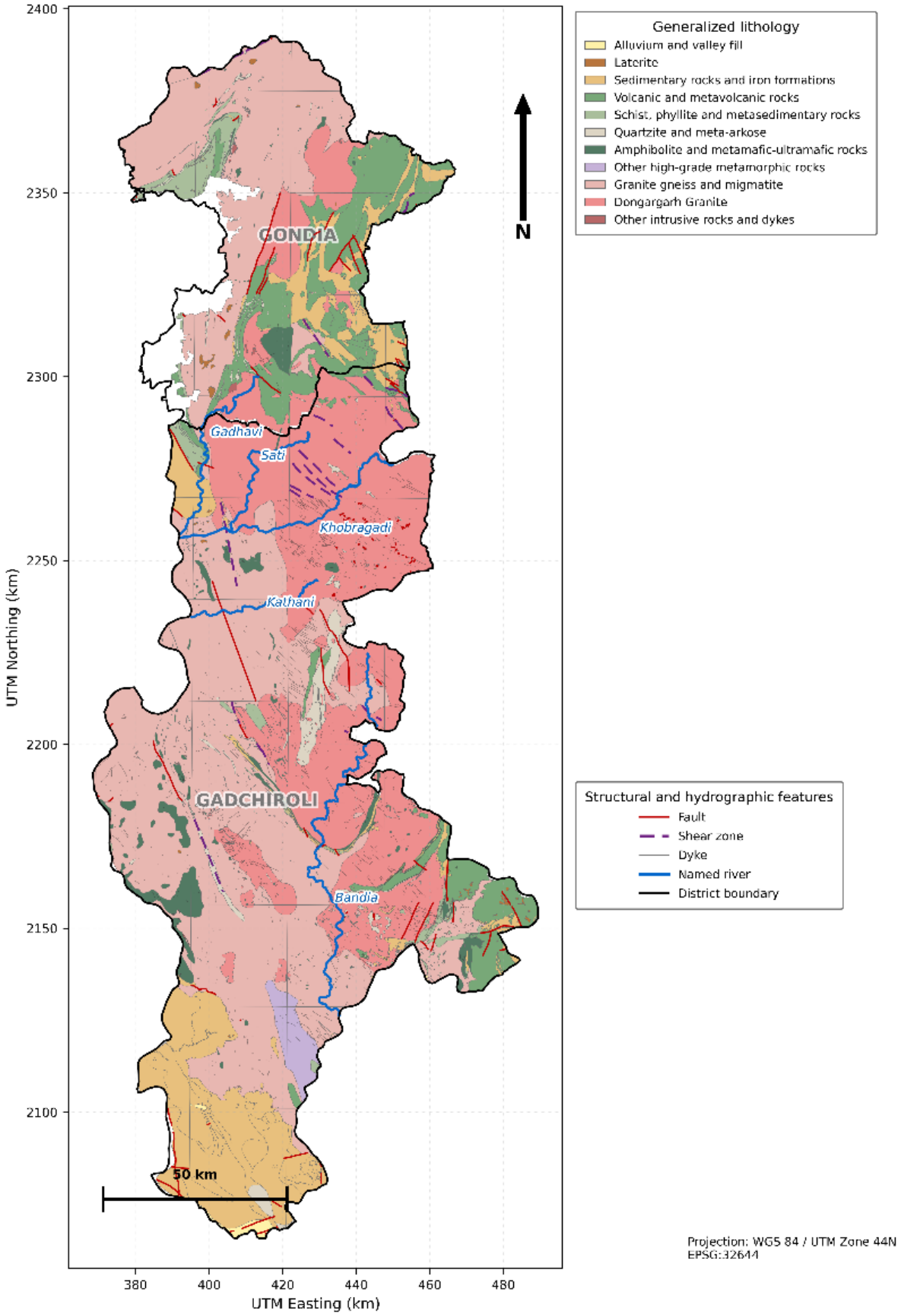


Figure 6. Geological and structural framework of Gondia and Gadchiroli districts, showing generalized lithological units, mapped faults, shear zones, dykes and studied rivers.

Table 3. Mapped structural characteristics of Gondia and Gadchiroli districts

District	Structure type	Mapped segments	Total mapped length (km)	Mean segment length (km)	Structural density (km/km²)
Gadchiroli	Dyke	1,873	1,563.60	0.835	0.1082
Gadchiroli	Fault	145	382.37	2.637	0.0265
Gadchiroli	Shear zone	20	151.13	7.556	0.0105
Gondia	Dyke	55	61.09	1.111	0.0112
Gondia	Fault	25	130.22	5.209	0.0238
Gondia	Shear zone	6	34.64	5.773	0.0063

The mapped abundance, total length and normalized density of faults, shear zones and dykes are compared in Table 3. Dykes were identified as the dominant structural class in Gadchiroli, whereas relatively similar fault densities were obtained for the two districts.

4.4 Drainage–Lithology Relationships and River-Wise Geological Associations

The spatial association between the extracted drainage network and the generalized lithological units is presented in Figure 7. Drainage channels were distributed across all major geological classes, although the greatest absolute channel lengths were recorded within granite gneiss and Dongargarh Granite because extensive portions of the mapped study area were occupied by these units. Drainage density was therefore used for the comparison of channel development after differences in lithological area had been accounted for.

Within Gadchiroli, the largest mapped lithological class was represented by granite, gneiss, and migmatite which covered 5,873.42 km² or 40.89% of the available geological coverage. A drainage length of 7,262.85 km and a drainage density of 1.237 km/km² were recorded within this unit. An area of 4,814.05 km² or 33.51% of the mapped district was occupied by Dongargarh Granite, within which 5,828.57 km of drainage and a density of 1.211 km/km² were recorded. Sedimentary rocks and iron formations occupied 13.33% of the mapped area and were associated with a drainage density of 1.115 km/km² (Table 4).

Lower drainage-density values were recorded over several less extensive geological units in Gadchiroli. Volcanic and metavolcanic rocks exhibited a density of 0.823 km/km², while quartzite and meta-arkose recorded 0.894 km/km². Schist, phyllite and metasedimentary rocks and other high-grade metamorphic rocks exhibited densities of 0.931 and 0.958 km/km², respectively. A relatively high value of 1.184 km/km² was obtained for alluvium and valley fill; however, this class represented only 0.33% of the mapped geological area. The lowest density was recorded over laterite at 0.526 km/km².

In Gondia, granite gneiss and migmatite also formed the largest mapped class, covering 2,191.31 km² or 43.41% of the geological coverage. Approximately 2,670.41 km of drainage occurred within this unit, producing a density of 1.219 km/km². Metavolcanic rocks occupied 25.25% of the mapped area and recorded a density of 1.118 km/km². Dongargarh Granite occupied a smaller mapped area of 719.25 km² but exhibited a drainage density of 1.271 km/km², which was the highest value among the spatially extensive lithological classes in Gondia.

An apparent density of 1.791 km/km² was obtained for other high-grade metamorphic rocks in Gondia. However, this unit covered only 0.95 km², and the calculated value was therefore influenced by a very small denominator. It was not treated as representative of district-scale drainage conditions. Similarly, densities obtained for minor laterite and intrusive-rock classes were interpreted cautiously because of their limited mapped extents.

Distinct lithological associations were exhibited by the studied rivers (Table 5). Geological coverage exceeding 95% was available for all five river alignments, thereby allowing their dominant geological settings to be compared. Dongargarh Granite was identified as the dominant lithology along four rivers, whereas the dominant unit along the Kathani River was represented by granite gneiss and migmatite. Gunwant G. Wadpalliwar. et. al(2024).

The strongest association with a single lithological class was exhibited by the Sati River. Its complete mapped alignment was covered by geological data, and approximately 45.10 km, or 91.98% of its length, was situated within Dongargarh Granite. Only 7.09% of its mapped length was associated with granite and gneiss. A strong association with Dongargarh Granite was also recorded for the Khobragadi River, for which 69.59% of the geologically covered length occurred within this unit and 29.97% occurred within granite and gneiss.

The Bandia River was distributed primarily across the two major granitoid classes. Of its mapped geological length, 54.95% was represented by Dongargarh Granite and 42.66% by granite gneiss and migmatite. In contrast, the Kathani River was dominated by granite gneiss and migmatite, which represented 69.83% of its mapped length, whereas approximately 30.00% of the alignment was represented by Dongargarh Granite.

The lowest dominant-lithology share was recorded for the Gadhavi River. Dongargarh Granite represented only 35.12% of its mapped geological length, while granite gneiss and migmatite accounted for 24.85%. The

remaining river length was distributed across sedimentary, and other geological units. Gadhavi was therefore identified as the most lithologically heterogeneous of the five river corridors.

The results demonstrated that drainage development and river alignments were distributed unevenly among the mapped geological units. However, the observed patterns were treated as spatial associations because drainage organization may also have been influenced by relief, weathering, soil characteristics and structural discontinuities.

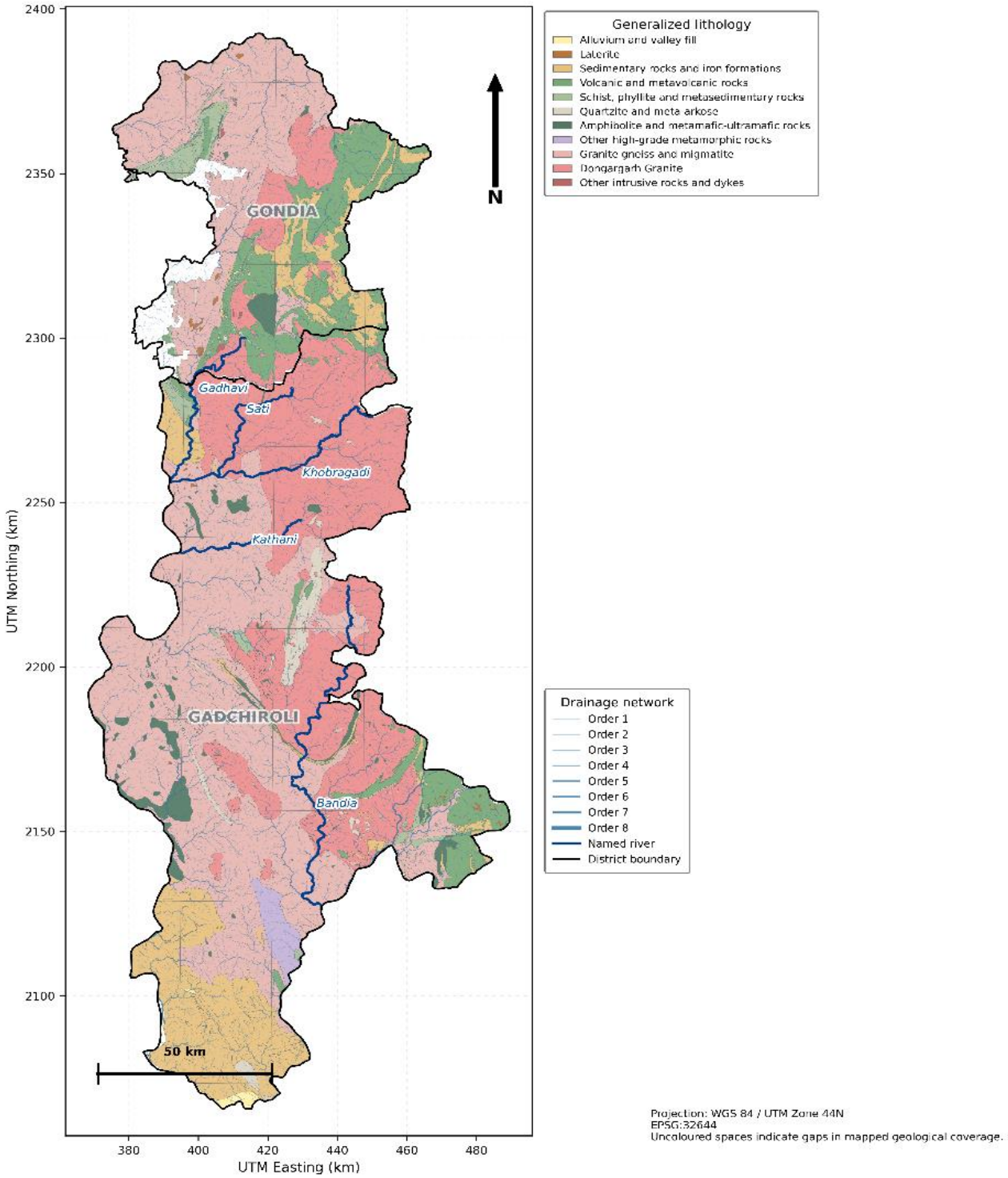


Figure 7. Spatial association of the Strahler-ordered drainage network and rivers with generalized lithological units in Gondia and Gadchiroli districts.

Table 4. Mapped lithological area, drainage length and drainage density by geological class.

District	Lithological class	Mapped area (km^2)	Mapped-area share (%)	Drainage length (km)	Drainage density (km/km^2)
Gadchiroli	Granite gneiss and with some migmatite	5,873.42	40.89	7,262.85	1.237
Gadchiroli	Dongargarh Granite	4,814.05	33.51	5,828.57	1.211
Gadchiroli	Sedimentary rocks and iron formations	1,915.06	13.33	2,136.16	1.115
Gadchiroli	Igneous and metavolcanic rocks	615.45	4.28	506.21	0.823
Gadchiroli	Amphibolite and metamafic-ultramafic rocks	416.47	2.90	482.18	1.158
Gadchiroli	Quartzite and meta-arkose	298.26	2.08	266.52	0.894
Gadchiroli	Other high-grade metamorphic rocks	200.39	1.40	192.03	0.958
Gadchiroli	Schist, phyllite and metasedimentary rocks	168.33	1.17	156.79	0.931
Gadchiroli	Alluvium and valley fill	47.13	0.33	55.78	1.184
Gadchiroli	Laterite	14.52	0.10	7.63	0.526
Gadchiroli	Other intrusive rocks and dykes	1.49	0.01	1.18	0.793
Gondia	Granite gneiss and migmatite	2,191.31	43.41	2,670.41	1.219
Gondia	Volcanic and metavolcanic rocks	1,274.61	25.25	1,425.46	1.118
Gondia	Dongargarh Granite	719.25	14.25	914.43	1.271
Gondia	Sedimentary rocks and iron formations	486.06	9.63	515.98	1.062
Gondia	Schist, phyllite and metasedimentary rocks	202.50	4.01	216.40	1.069
Gondia	Amphibolite and metamafic-ultramafic rocks	90.88	1.80	83.64	0.920
Gondia	Quartzite and meta-arkose	51.50	1.02	26.12	0.507
Gondia	Laterite	19.63	0.39	23.41	1.193
Gondia	Other intrusive rocks and dykes	10.69	0.21	9.32	0.872
Gondia	Other high-grade metamorphic rocks	0.95	0.02	1.70	1.791

Lithology-specific drainage characteristics are summarized in Table 4. Drainage length was normalized by the mapped area of each geological class to allow comparison among lithological units of substantially different spatial extent.

Table 5. Dominant lithological associations of the Studied rivers

River	Total river length (km)	Length within mapped geology (km)	Geological coverage (%)	Dominant lithology	Dominant lithology length (km)	Dominant share (%)	Second-ranked lithology	Second-ranked share (%)
Bandia	138.27	137.20	99.23	Dongargarh Granite	75.39	54.95	Granite gneiss and Migmatite	42.66
Khobragadi	79.89	78.24	97.94	Dongargarh Granite	54.45	69.59	Granite gneiss	29.97
Gadhavi	68.49	65.46	95.58	Dongargarh Granite	22.99	35.12	Granite gneiss	24.85
Sati	49.03	49.03	100.00	Dongargarh Granite	45.10	91.98	Granite gneiss	7.09
Kathani	44.42	44.42	100.00	Granite gneiss and migmatite	31.02	69.83	Dongargarh Granite and Migmatite	30.00

River-wise lithological associations are presented in Table 5. The results identify the dominant and second-ranked lithologies along each river while accounting for the proportion of each river covered by the geological dataset.

4.5 Drainage–Structure Intersections and Studied-River Crossing Patterns

Numerous spatial intersections were identified between the extracted drainage network and the mapped faults, shear zones and dykes. Considerably higher crossing counts were recorded in Gadchiroli than in Gondia, particularly for dyke intersections (Table 6). This difference corresponded with the substantially greater mapped dyke length and density previously identified in Gadchiroli. A total of 932 drainage–dyke intersections were recorded in Gadchiroli, corresponding to 5.472 crossings per 100 km of drainage. By comparison, only 28 drainage–dyke intersections were identified in Gondia, resulting in a normalized rate of 0.441 crossings per 100 km. The dyke-crossing rate was therefore more than twelve times higher in Gadchiroli than in Gondia.

Fault intersections were more evenly distributed between the two districts after normalization. In Gadchiroli, 291 drainage–fault crossings were recorded, equivalent to 1.709 crossings per 100 km of drainage. Gondia contained 81 fault crossings, corresponding to 1.276 crossings per 100 km. Although the raw number of fault intersections was substantially greater in Gadchiroli, the normalized difference between the districts was comparatively limited. Shear-zone crossings formed the least frequent drainage–structure intersection category. A total of 121 shear-zone crossings was recorded in Gadchiroli, producing a normalized rate of 0.710 crossings per 100 km. In Gondia, 18 crossings were identified, equivalent to 0.284 crossings per 100 km.

A substantial proportion of structural intersections occurred along first-order channels. First-order streams accounted for 47.64% of dyke crossings, 45.02% of fault crossings and 49.59% of shear-zone crossings in Gadchiroli. In Gondia, the corresponding proportions were 64.29%, 59.26% and 44.44%, respectively. However, these values were interpreted cautiously because first-order streams represented approximately half of all extracted drainage segments. Therefore, the observed first-order dominance could not independently be regarded as evidence of preferential structural control. Mapped structures were also intersected by higher-order channels. In Gadchiroli, dyke intersections extended to eighth-order channels, while fault and shear-zone intersections reached seventh and sixth orders, respectively. In Gondia, faults were intersected by channels up to fifth order, dykes up to fourth order and shear zones up to seventh order. Spatial coincidence was therefore observed across both tributary and trunk-channel components of the drainage network.

The distribution of structural intersections along the five studied rivers is presented in Figure 8 and Table 7. A total of 40 mapped structural crossings was identified along the combined river network. Of these, 32 crossings, or 80%, were associated with dykes, while five were associated with faults and three with shear zones. Bandia recorded the greatest number of structural intersections, with 23 crossings along a mapped length of 138.27 km. The corresponding normalized rate was 16.635 crossings per 100 km, which was the highest among the five rivers. This result was dominated by 20 dyke crossings, equivalent to 14.465 dyke crossings per 100 km. Two fault crossings and one shear-zone crossing were also identified along Bandia.

Sati displayed the second-highest normalized total crossing rate, with six intersections and a rate of 12.237 crossings per 100 km. All six crossings were associated with dykes; no mapped fault or shear-zone crossing was identified along the analysed river alignment. Kathani recorded three structural intersections, comprising one fault crossing and two dyke crossings. Its total normalized rate was 6.753 crossings per 100 km. The fault-crossing rate of 2.251 per 100 km was based on a single intersection and was therefore interpreted cautiously.

Gadhavi contained four structural crossings, equally divided between faults and dykes. The total normalized crossing rate was 5.841 per 100 km. Its fault-crossing rate of 2.920 per 100 km was the highest among the five rivers, although it was based on only two mapped intersections. Four structural crossings were recorded along Khobragadi, producing a normalized rate of 5.007 crossings per 100 km. No fault crossing was identified. Two shear-zone and two dyke crossings were recorded, each corresponding to 2.503 crossings per 100 km. Khobragadi was the only river for which shear-zone crossings equalled dyke crossings.

Spatial coincidence between mapped structural features and the drainage system was demonstrated by the crossing analysis. However, the intersections were not interpreted as independent proof of tectonic control, fault-guided channel development or contemporary channel deformation. Crossing frequency was also recognized as being influenced by river length, drainage-network density and the spatial abundance of mapped structural features.

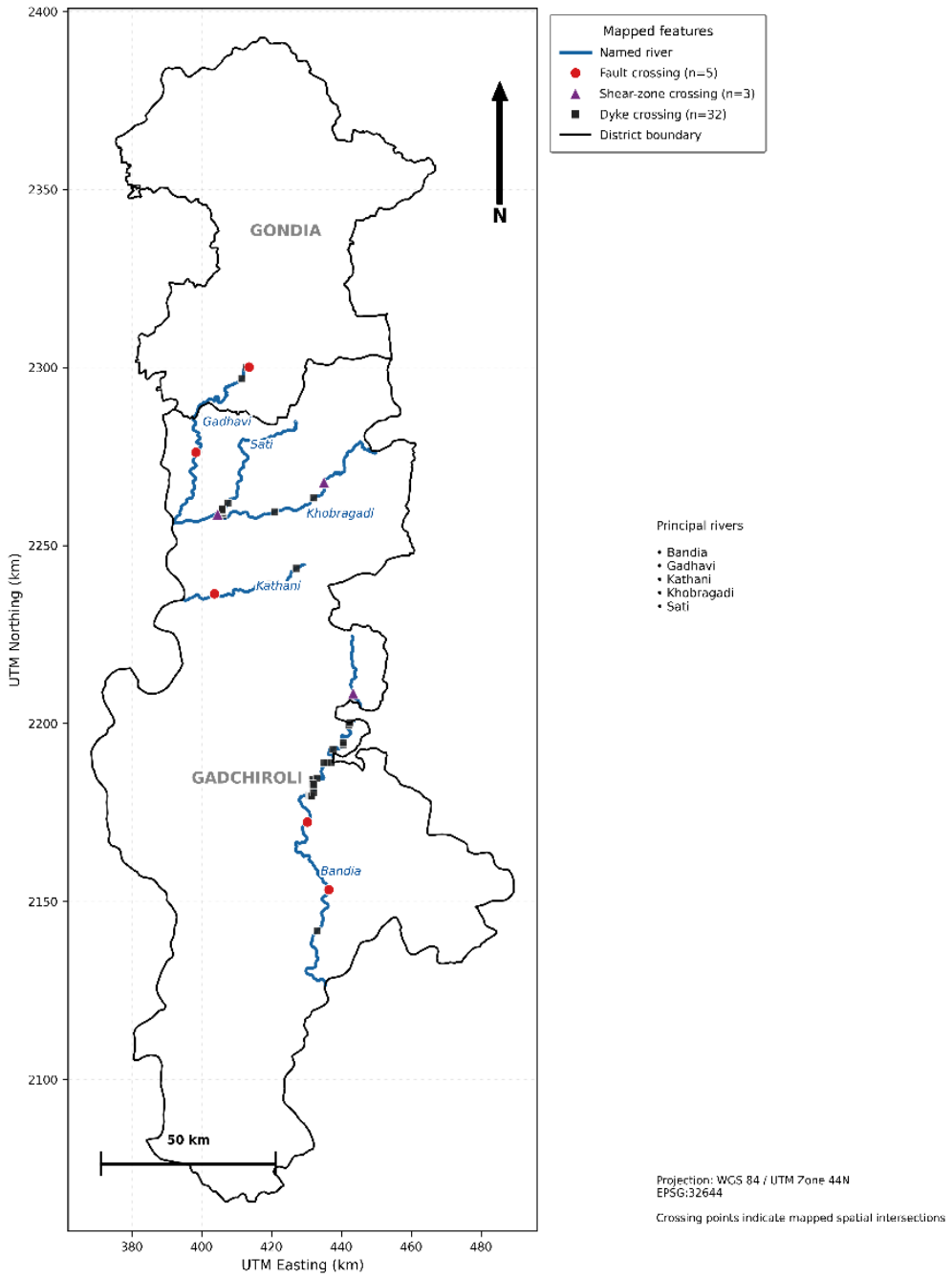


Figure 8. Spatial distribution of mapped fault, shear-zone and dyke crossings along the studied rivers of Gondia and Gadchiroli districts.

Table 6. Intersections between the district-scale drainage network and mapped structural features

District	Structure type	Crossing count	Crossings per 100 km of drainage	First-order crossings	First-order share (%)	Highest crossed stream order
Gadchiroli	Dyke	932	5.472	444	47.64	8
Gadchiroli	Fault	291	1.709	131	45.02	7
Gadchiroli	Shear zone	121	0.710	60	49.59	6
Gondia	Dyke	28	0.441	18	64.29	4
Gondia	Fault	81	1.276	48	59.26	5
Gondia	Shear zone	18	0.284	8	44.44	7

District-scale drainage–structure intersections are summarized in Table 6. Both raw crossing counts and rates normalized per 100 km of drainage are reported so that differences in total network length between Gondia and Gadchiroli can be accounted for.

Table 7. Raw and normalized structural crossings along the studied rivers.

River	River length (km)	Fault crossings	Fault crossings per 100 km	Shear-zone crossings	Shear-zone crossings per 100 km	Dyke crossings	Dyke crossings per 100 km	Total structural crossings	Total crossings per 100 km
Bandia	138.27	2	1.446	1	0.723	20	14.465	23	16.635
Khobragadi	79.89	0	0.000	2	2.503	2	2.503	4	5.007
Gadhavi	68.49	2	2.920	0	0.000	2	2.920	4	5.841
Sati	49.03	0	0.000	0	0.000	6	12.237	6	12.237
Kathani	44.42	1	2.251	0	0.000	2	4.502	3	6.753

Structural crossings along the five studied rivers are compared in Table 7. River-wise comparison is enabled by the length-normalized rates, through which the predominance of dyke intersections, particularly along the Bandia and Sati rivers, is demonstrated.



Fig 9.a Gondia, Deori, Dhasgarh, Metavolvanics,



Fig 9.b.Gondia, Deori, Sedimentary: Conglomerate

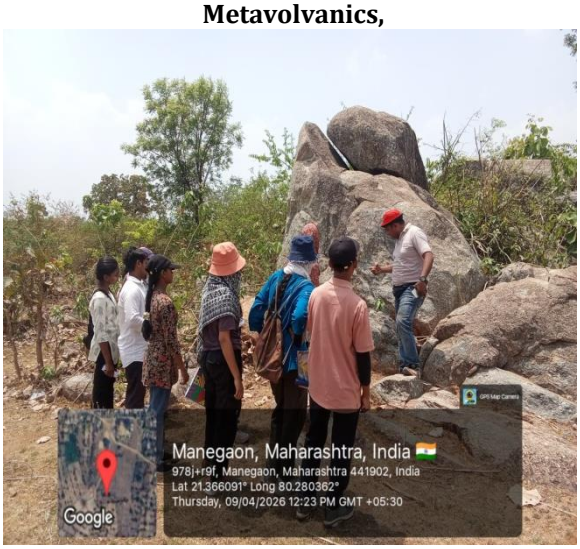


Fig 9.c Gondia, Amgaon Gneiss



Fig 9.d Gadchiroli, , Dongargarh Granite with Fault



Fig 9.e Gadchiroli, Dibhana Gneiss &Migmatite



Fig 9.f Gadchiroli, Armori, Quartzite and BIF

Fig: 9 Field work for the validation of Remote Sensing data

5. DISCUSSION

The drainage systems of Gondia and Gadchiroli were developed across heterogeneous terrain characterized by contrasting elevations, slopes, lithological units and mapped structural features. Although substantial differences in area and relief were present, only a limited difference in drainage density was observed. Drainage densities of 1.179 and 1.160 km/km^2 were recorded for Gadchiroli and Gondia, respectively. The considerably greater total drainage length in Gadchiroli was therefore associated mainly with its larger geographical extent rather than with a fundamentally denser drainage network. This interpretation is consistent with the principle that drainage density must be evaluated relative to mapping scale, contributing area and network-extraction criteria rather than through absolute channel length alone (Amatulli et al., 2022; Lin et al., 2021). Nevertheless, a more topographically variable landscape was indicated in Gadchiroli by the wider elevation range and the higher mean and maximum slopes.

It was demonstrated by the terrain maps that steep and strongly dissected sectors were concentrated mainly in eastern and southern Gadchiroli and in localized parts of Gondia. Spatial correspondence was observed between closely spaced contours, steep slope classes, ridge systems and dissected uplands, whereas gentler gradients were associated with broader low-relief surfaces. Local channel initiation and flow concentration may have been influenced by these terrain contrasts. Terrain derivatives and morphometric indicators have frequently been applied to the evaluation of watershed dissection and surface-water routing in GIS-based studies, although geological and environmental conditions must also be considered during interpretation (Pande et al., 2021; Singh et al., 2023). The similar district-scale drainage densities indicate that the drainage pattern could not be explained by terrain alone. Drainage development must therefore be interpreted in relation to the combined effects of lithology, weathering, structural discontinuities and topographic gradients.

The drainage hierarchy was strongly dominated by first- and second-order channels in both districts. Approximately three-quarters of the total segment count and drainage length were represented by these two stream orders. Comparable branching structures were indicated by the similarity of these proportions despite differences in district size and geological composition. Numerous lower-order tributaries were progressively integrated into fewer higher-order channels, consistent with the hierarchical network organization described by the Strahler stream-order system (Strahler, 1957). The eighth-order network identified in Gadchiroli, compared with the seventh-order network in Gondia, was consistent with the larger drainage extent of Gadchiroli. However, maximum stream order should not be treated independently as evidence of greater erosional activity or structural control because stream hierarchy is affected by basin extent, DEM resolution, hydrological conditioning and the selected extraction threshold (O'Callaghan & Mark, 1984; Lindsay, 2016; Shekar & Mathew, 2024).

It was demonstrated by the lithological analysis that granite gneiss–migmatite and Dongargarh Granite formed the principal geological settings of the mapped drainage network. In Gadchiroli, drainage densities of approximately 1.237 and 1.211 km/km^2 were recorded over granite gneiss–migmatite and Dongargarh Granite, respectively. In Gondia, a density of 1.271 km/km^2 was recorded over Dongargarh Granite, whereas 1.219 km/km^2 was obtained over granite gneiss–migmatite. Well-developed drainage networks were therefore identified across the extensive granitoid terrains of both districts. Nevertheless, drainage density cannot be attributed solely to bedrock type. It has been emphasized in morphometric reviews that drainage density is jointly affected by relief, weathering, soils, vegetation, rainfall, source resolution and extraction procedures (Shekar & Mathew, 2024). The observed lithology-specific differences may therefore also have been influenced by variations in weathering depth, joint density, regolith characteristics, slope and structural fabric.

Distinct geological associations were exhibited by the studied rivers. Strong associations with Dongargarh Granite were recorded for Sati and Khobragadi, whereas Kathani was aligned primarily across granite gneiss and migmatite. Bandia was distributed across both major granitoid classes, while the most lithologically diverse corridor was traversed by Gadhavi. The alignment of Gadhavi across several lithological boundaries, rather than within a single rock unit, is suggested by this greater geological diversity. The need for spatially explicit analysis is reinforced by such river-wise variation because multiple geological and topographic domains may be traversed by regional hydrographic networks (Lehner & Grill, 2013; Yamazaki et al., 2019). These associations were nevertheless treated as spatial relationships and not as independent evidence that river courses were determined by lithology alone.

The most extensive mapped structural class was represented by dykes, particularly in Gadchiroli, where substantially greater dyke density and drainage–dyke crossing frequency were recorded than in Gondia. More comparable fault-crossing rates were obtained between the districts, whereas relatively few shear-zone crossings were identified. At the river scale, high normalized dyke-crossing rates were recorded along Bandia and Sati, the highest normalized fault-crossing rate was obtained for Gadhavi, and mapped shear-zone intersections were distinguished along Khobragadi. Spatial coincidence between drainage alignments and structural features was therefore indicated by these patterns. However, channel initiation, redirection or maintenance by a particular structure cannot be demonstrated by a geometric intersection alone. Some crossings may instead have been produced by the

abundance, mapped length and orientation of structural features.

The high proportion of crossings involving first-order streams must also be interpreted cautiously. Approximately half of the extracted network was represented by first-order channels, and a greater statistical likelihood of intersection with mapped structural features was therefore present. First-order crossing frequency cannot be used independently as evidence of structural control because of this numerical dominance. This caution is consistent with broader morphometric guidance under which stream-order and segment-frequency statistics are interpreted within the topology and extraction scale of the mapped network (Strahler, 1957; Shekar & Mathew, 2024). A more definitive interpretation would require directional analysis of channel and structural orientations, field confirmation of fracture-controlled valleys and evaluation of whether mapped structures are systematically followed, crossed or terminated against by channels.

A basis for discussing possible groundwater-recharge implications was also provided by the results, although recharge was not directly estimated. Integrated geospatial approaches are widely applied to the identification of terrain and geological conditions relevant to water-resource assessment and groundwater planning (Jagadeesha & Manavalan, 2025; Pande et al., 2021; Tarate et al., 2024). In crystalline terrain, potential settings for infiltration and subsurface water movement may be provided by weathered granitoid surfaces, valley floors, footslope positions and hydraulically connected faults or shear zones. Locations requiring further hydrogeological investigation may similarly be indicated by river–structure intersections, particularly where fractures remain open and connected with weathered material.

However, mapped structures cannot automatically be classified as recharge zones. Groundwater movement may be locally restricted by massive dykes, whereas permeability may be enhanced along fractured dyke margins and weathered contacts. Rapid surface-water transfer may be promoted by steep slopes and dense drainage, although localized infiltration may still be permitted by fractured bedrock beneath such terrain. Greater infiltration may be suggested by lower drainage density in some settings, yet similar values may also be produced by low relief, geological resistance or drainage-extraction effects. Groundwater recharge should therefore not be inferred independently from drainage density, lithology or structural crossings.

The groundwater implications should consequently be regarded as conceptual. Reliable recharge assessment would require rainfall, evapotranspiration, soil and land-cover information, regolith thickness, aquifer properties, groundwater-level observations and field validation. Preliminary identification of hydrogeologically relevant locations can be supported by geospatial analysis, but direct hydrological and aquifer measurements cannot be replaced by it (Jagadeesha & Manavalan, 2025; Tarate et al., 2024). Candidate settings for further investigation, rather than confirmed groundwater-potential areas, are therefore identified by the present results. Overall, drainage organization in Gondia and Gadchiroli was interpreted as the combined expression of terrain, lithological variability, weathering and mapped structural heterogeneity, with no single factor being sufficient to provide a complete explanation.

6. CONCLUSION

The relationships among terrain, drainage organization, lithology and mapped structural features across Gondia and Gadchiroli districts were evaluated using NASADEM topographic data, district-scale drainage extraction and geological information. A wider elevation range, steeper relief and a larger drainage network were identified in Gadchiroli than in Gondia. However, similar drainage densities were obtained for both districts, indicating that the greater channel length in Gadchiroli was influenced by its larger geographical extent rather than by a denser drainage system. The extracted network was dominated by first- and second-order streams, by which approximately three-quarters of the total segment count and drainage length were represented. Similar drainage-network development across the two districts, despite differences in terrain and geology, was suggested by this comparable hierarchical organization. Granite gneiss–migmatite and Dongargarh Granite were identified as the principal lithological settings of the drainage system. Through river-wise analysis, strong associations with Dongargarh Granite were recorded for Sati and Khobragadi, a predominant alignment across granite gneiss and migmatite was identified for Kathani, and the most lithologically diverse corridor was identified along Gadhavi.

Spatial intersections with the drainage network were exhibited by mapped dykes, faults and shear zones. Dyke crossings were recorded especially frequently in Gadchiroli, whereas comparatively similar fault-crossing rates were obtained for the two districts. High normalized dyke-crossing rates were recorded along Bandia and Sati, the highest normalized fault-crossing rate was obtained for Gadhavi, and shear-zone intersections were distinguished along Khobragadi. Spatial association was demonstrated by these findings, but tectonic control was not proven. Drainage organization was interpreted as being jointly influenced by relief, lithological variation, weathering and structural heterogeneity. Conditions potentially favourable for groundwater infiltration may be provided by weathered granitoid zones, valley settings and hydraulically connected fractures. Nevertheless, groundwater recharge was not measured directly, and no groundwater-potential map was produced. In future work, rainfall, soils, regolith thickness, groundwater

levels, aquifer properties and field validation should be incorporated so that the identified hydrogeological implications can be tested.

REFERENCES

Amatulli, G., Garcia Marquez, J., Sethi, T., Kiesel, J., Grigoropoulou, A., Üblacker, M., … Domisch, S. (2022). Hydrography90m: A new high-resolution global hydrographic dataset. Earth System Science Data, 14, 4525–4550. https://doi.org/10.5194/essd-14-4525-2022

Drusch, M., Del Bello, U., Carlier, S., Colin, O., Fernandez, V., Gascon, F., Hoersch, B., Isola, C., Laberinti, P., Martimort, P., Meygret, A., Spoto, F., Sy, O., Marchese, F., & Bargellini, P. (2012). Sentinel-2: ESA's optical high-resolution mission for GMES operational services. Remote Sensing of Environment, 120, 25–36. https://doi.org/10.1016/j.rse.2011.11.026

Geofabrik GmbH. (2026). OpenStreetMap data extract for Western Zone, India [GeoPackage dataset]. Geofabrik Download Server. https://download.geofabrik.de/asia/india/western-zone.html

Gorelick, N., Hancher, M., Dixon, M., Ilyushchenko, S., Thau, D., & Moore, R. (2017). Google Earth Engine: Planetary-scale geospatial analysis for everyone. Remote Sensing of Environment, 202, 18–27. https://doi.org/10.1016/j.rse.2017.06.031

Gunwant G. Wadpalliwar., Sapana P. Titirmare., Riya K. Kapkar and Samir B. Deshmukh. (2024). Morphometric Analysis of Gadhvi River, Sub-Basin Using Remote Sensing and GIS techniques. Gondwana Geological Society, Geosciences and Sustainable Development in Trible Areas, Vol. 3, 81-91. https://www.researchgate.net/publication

Gunwant G. Wadpalliwar., Samir B. Deshmukh. Raju G. Munghate. And Abhijeet P. Dharashiwkar (2024). Application of morphometric Study For Groundwater Management In Dongargarh Granite Around Kurkheda, District Gadchiroli, Maharashtra. International Research Journal of Management Science & Technology. Vol 15 Issue 3, 30-42. ISSN 2250 – 1959 (0nline) 2348 – 9367 (Print) http://www.irjmst.com

Hou, Z., Zheng, D., Xiang, F., Bai, J., Chen, A., Ma, C., & Hou, M. (2025). Application of HydroSHEDS dataset in climate change and biodiversity evolution. Geological Journal of China Universities, 31(2), 238. https://doi.org/10.16108/j.issn1006-7493.2024023

Jagadeesha, C. J., & Manavalan, P. (2025). Advancing the use of geoinformatics-based water management. In Remote Sensing, GIS and Modelling for Water Resource Management: Volume 2 (pp. 509–535). Springer Nature Switzerland.

Lehner, B., & Grill, G. (2013). Global river hydrography and network routing: Baseline data and new approaches to study the world's large river systems. Hydrological Processes, 27(15), 2171–2186. https://doi.org/10.1002/hyp.9740

Lin, P., Pan, M., Wood, E. F., Yamazaki, D., & Allen, G. H. (2021). A new vector-based global river network dataset accounting for variable drainage density. Scientific Data, 8, 28. https://doi.org/10.1038/s41597-021-00819-9

Lindsay, J. B. (2016). Whitebox GAT: A case study in geomorphometric analysis. Computers & Geosciences, 95, 75–84. https://doi.org/10.1016/j.cageo.2016.07.003

Liu, Y., Wang, J., Liu, C., Huang, Y., Liu, Y., Liu, J., … Qu, W. (2026). An improved global river vector dataset based on multi-source river data fusion. Scientific Data, 13, 88. https://doi.org/10.1038/s41597-025-06399-2

Monteiro, E. S. V., & Patrício, G. R. (2024). Analysing temporal evolution of OpenStreetMap waterways completeness in a mountain region of Portugal. Remote Sensing, 16(17), 3159. https://doi.org/10.3390/rs16173159

NASA Jet Propulsion Laboratory. (2020). NASADEM merged DEM global 1 arc second V001 [Data set]. NASA EOSDIS Land Processes Distributed Active Archive Center. https://doi.org/10.5067/MEASURES/NASADEM/NASADEM_HGT.001

O'Callaghan, J. F., & Mark, D. M. (1984). The extraction of drainage networks from digital elevation data. Computer Vision, Graphics, and Image Processing, 28(3), 323–344. https://doi.org/10.1016/S0734-189X(84)80011-0

Pande, C. B., Moharir, K. N., & Khadri, S. F. R. (2021). Watershed planning and development based on morphometric analysis and remote sensing and GIS techniques: A case study of a semi-arid watershed in Maharashtra, India. In C. B. Pande and K. N. Moharir (Eds.), Groundwater Resources Development and Planning in the Semi-Arid Region (pp. 199–220). Springer. https://doi.org/10.1007/978-3-030-68124-1_11

Pekel, J.-F., Cottam, A., Gorelick, N., & Belward, A. S. (2016). High-resolution mapping of global surface water and its long-term changes. Nature, 540, 418–422. https://doi.org/10.1038/nature20584

Pierson, M., & Mehrabi, Z. (2024). Mapping waterways worldwide with deep learning. arXiv.

https://doi.org/10.48550/arXiv.2412.00050

S.B. Deshmukh ,A.M. Pophare., Y.A. Murkute. and G.G. Wadpalliwar (2023). Geochemical Characteristics of Mafic Dykes from Wairagarh Area, Western Bastar Craton, Central India. Journal of Geosciences Research. Vol. 8, No.2, July, 2023, pp. 133-141 https://www.researchgate.net/publication

Shekar, P. R., & Mathew, A. (2024). Morphometric analysis of watersheds: A comprehensive review of data sources, quality, and geospatial techniques. Watershed Ecology and the Environment, 6, 13–25. https://doi.org/10.1016/j.wsee.2023.12.001

Singh, M. C., Satpute, S., & Prasad, V. (2023). Remote sensing and GIS-based watershed prioritization for land and water conservation planning and management. Water Science & Technology, 88(1), 233–265. https://doi.org/10.2166/wst.2023.207

Strahler, A. N. (1957). Quantitative analysis of watershed geomorphology. Transactions, American Geophysical Union, 38(6), 913–920. https://doi.org/10.1029/TR038i006p00913

Tarate, S. B., Patel, N. R., Danodia, A., Pokhariyal, S., & Parida, B. R. (2024). Geospatial technology for sustainable agricultural water management in India—A systematic review. Geomatics, 4(2), 91–123. https://doi.org/10.3390/geomatics4020006

Xu, H. (2006). Modification of normalised difference water index to enhance open-water features in remotely sensed imagery. International Journal of Remote Sensing, 27(14), 3025–3033. https://doi.org/10.1080/01431160600589179

Yamazaki, D., Ikeshima, D., Sosa, J., Bates, P. D., Allen, G. H., & Pavelsky, T. M. (2019). MERIT Hydro: A high-resolution global hydrography map based on latest topography dataset. Water Resources Research, 55(6), 5053–5073. https://doi.org/10.1029/2019WR024873

Yuan, S., Liang, X., Lin, T., Chen, S., Liu, R., Wang, J., … Gong, P. (2025). A comprehensive review of remote sensing in wetland classification and mapping. arXiv. https://doi.org/10.48550/arXiv.2504.10842